RESEARCH PAPER

Green synthesis of gold nanoparticles from *Stachytarpheta jamaicensis*: An eco-friendly approach with promising anticancer potency

Firli Rahmah Primula Dewi [1]*, Sri Puji Astuti Wahyuningsih [1], Suat Cheng Tan [2], Vuanghao Lim [3], Arniza Khairani Mohd Jamil [4], Nor Saadah Mohd Yusof [4], P. Muthu [5], Ufairanisa Islamatasya [1]

[1]Department of Biology, Faculty of Science and Technology, Universitas Airlangga, Indonesia
[2]School of Health Sciences, Health Campus, Universiti Sains Malaysia, 16150 Kubang Kerian, Kelantan, Malaysia
[3]Advanced Medical and Dental Institute, Universiti Sains Malaysia, Bertam, Penang, Malaysia
[4]Department of Chemistry, Faculty of Science, Universiti Malaya, Malaysia
[5]Department of Biomedical Engineering, SRM Institute of Science and Technology, Kattankulathur, Tamilnadu, India

ABSTRACT

Objective(s): Green synthesis of gold nanoparticles (AuNPs) using plant extracts has gained significant attention for its eco-friendly approach and potential therapeutic applications. In this study, we present the green synthesis of AuNPs utilizing *Stachytarpheta jamaicensis* extract, exploring its potency for anticancer therapy.

Materials and Methods: The synthesized AuNPs were characterized using various techniques, including UV-Vis spectroscopy, Fourier Transform-Infrared (FT-IR), Scanning Electron Microscope (SEM), and Particle Size Analyzer (PSA). The anticancer potency of AuNPs was examined by MTT assay in the breast cancer (MCF7) cell line, along with gene expression analysis of two oncogenes, c-Myc (*MYC*) and Cyclin D1 (*CCND1*).

Results: The formation of AuNPs was proven by SEM with an average particle size of 60.3 nm. FTIR analysis elucidated the plant extract components responsible for the reduction and stabilization processes during AuNP synthesis, affirming the involvement of multiple compounds from *S. jamaicensis* extract. Cytotoxicity assessments in the MCF7 cell line demonstrated a substantial reduction in cell viability, yielding an IC50 value of 19.53 µg/mL. The downregulation of *MYC* and *CCND1* following AuNP treatment hinted at a potential mechanism underpinning the observed decrease in cell viability.

Conclusion: Our findings significantly contribute to the evolving body of evidence advocating for the use of green-synthesized AuNPs from *S. jamaicensis* extract as promising contenders in anticancer therapy. Emphasizing their potential in targeted cancer treatment strategies, this study underscores the importance of environmentally conscious approaches in nanomedicine development.

Keywords: *Metal nanoparticles, Nanomedicine, Neoplasms, Oncogenes, Plant extracts*

How to cite this article
Dewi FRP, Wahyuningsih SPA, Tan SCh, Lim V, Jamil AKM, Yusof NSM, Muthu P, Islamatasya U. Green Synthesis of Gold Nanoparticles from Stachytarpheta jamaicensis: An Eco-Friendly Approach with Promising Anticancer Potency. Nanomed J. 2025; 12(1): 51-58. DOI: 10.22038/nmj.2024.77277.1883

INTRODUCTION

Gold nanoparticles (AuNPs) have garnered considerable attention due to their versatile applications [1-3]. Due to their small size, these particles have the ability to penetrate tissues and target immune cells, including lymphoid tissues. This characteristic makes them potentially valuable in applications such as immunotherapy, drug delivery, and anticancer therapy. Moreover, AuNPs are recognized for their potential utility as nano-sensors, biomarkers, colorimetric sensors, antibacterial agents, and antioxidants [4-6]. These nanoparticles can be easily synthesized, offering high chemical and thermal stability [7]. However, conventional physical and chemical synthesis methods, despite their efficacy, have drawbacks concerning environmental impact and potential hazards to human health, limiting their applicability in sensitive fields such as food and

* *Corresponding author: Email: firli.rahmah@fst.unair.ac.id*
Note. This manuscript was submitted on January 4, 2024; approved on February 12, 2024

medicine [8].

In response to the demand for sustainable practices, researchers have shifted their focus to develop safer methods for AuNP synthesis. Among these methods, the utilization of biological systems, including microbes, fungi, and plant extracts, has gained prominence [9-11]. In contrast to the challenges encountered in microbe-assisted synthesis [11], the process of plant-mediated ones is gaining more attention due to its ease of handling and the ability to control the size and shape of NPs. Phytochemicals such as flavonoids, polyphenols, and alkaloids play pivotal roles in the reduction of gold ions, leading to the formation of stable and biocompatible AuNPs. Plant-mediated synthesis of AuNPs stands out for its simplicity, rapid synthesis rate, eco-friendliness, and the potential enhancement of biocompatibility with biomolecules [10, 12, 13]. One of the most compelling aspects of green-synthesized AuNPs lies in their potential for anticancer therapy [14-16]. AuNPs have demonstrated inherent cytotoxic effects on cancer cells while sparing normal cells, making them ideal candidates for targeted drug delivery and localized therapy [17-19]. The biocompatible nature of plant-synthesized AuNPs further enhances their compatibility within biological systems, fostering the development of novel strategies for cancer treatment with reduced side effects [17].

Stachytarpheta jamaicensis (L.) Vahl, belonging to the Verbenaceae family, predominantly flourishes in tropical regions of the Americas and subtropical forests spanning Africa, Asia, and Oceania [20]. This herbaceous plant, considered weedy, reaches a height of 60–120 cm and is distinguished by a smooth, dark green stem that transitions to a woody base. *S. jamaicensis* boasts a rich content of secondary metabolites, including alkaloids, flavonoids, phenols, steroids, and terpenoids. Notably, the phenolic compounds, consisting of coumarins, flavonoids, tannins, and saponins, have been extensively investigated for their therapeutic attributes. Among these, the phytochemicals in the phenolic compounds of *S. jamaicensis*, incorporating coumarins, flavonoids, tannins, and saponins, have garnered considerable attention from researchers due to their therapeutic potential. This plant, renowned in herbal medicine, is acknowledged for a diverse array of properties, including antacid, analgesic [21], anti-inflammatory [22], hypotensive [23], diuretic, laxative, sedative, and spasmogenic.

Building upon prior research on the biosynthesis of AuNPs [24, 25], this study is the first to introduce the green synthesis of AuNPs utilizing *S. jamaicensis* leaf extract. The synthesized AuNPs underwent comprehensive characterization through UV–visible Spectroscopy, Fourier Transformed Infrared Spectroscopy (FT-IR), Scanning Electron Microscopy (SEM), and Particle Size Analyzer (PSA). The anticancer potential of AuNPs formulated with *S. jamaicensis* leaf extract was explored against the MCF7 breast cancer cell line, along with an assessment of the mRNA levels of Cyclin-D1 and c-Myc, two influential oncogenes associated with breast cancer.

MATERIALS AND METHODS

Preparation of S. jamaicensis leaf extract

Fresh *S. jamaicensis* leaves were collected from the author's private collection. The leaves were washed once with tap water and twice with double-distilled water. The *S. jamaicensis* leaves (7 g) were finely diced and mixed with 35 mL of $ddH_{2O.}$ The mixture was then stirred and heated for 60 min at 55 °C. The mixture was then centrifuged and filtered through Whatman No. 1 filter paper to obtain the aqueous extract [26].

Synthesis of AuNPs

Gold ion solution was prepared by dissolving 20 mg of $HAuCl_4$ (Smart Lab, Indonesia) with 20 mL of ddH_2O to form a 1 g/L solution. AuNPs were prepared by mixing 20 mL of gold ion solution with 20 mL of plant extract. The mixture were then incubated for 24 hr at room temperature in dark conditions. The mixture color changed to a deep purple due to the formation of AuNPs.

Characterization of AuNPs

The reduction of AuNPs was verified through UV-Vis spectroscopy, conducted at 2 nm intervals within the range of 400–700 nm. Identification of the bioreduction compounds involved in the reaction was carried out using FT-IR, specifically with the Bruker Alpha II ECO-ATR system covering the range of 450–4000 cm−1. AuNPs positioned on the surface of the Attenuated Total Reflection (ATR) SURFACE, underwent spectral analysis through scanning at a defined resolution. The OPUS software facilitated the analysis of spectral data, aligning it with available reference databases of spectra. For size distribution determination in the liquid phase, PSA characterization was employed. This method was commenced with an analysis of refractive index and viscosity in the test samples and was crucial for understanding NP properties like chemical receptivity, stability, and biocompatibility. Subsequently, 2 mL of sample was introduced into a PSA analysis cuvette, where a laser beam was emitted into the sample, and the intensity of the reflected light was measured to ascertain particle size and distribution [27, 28].

The AuNPs emulsion underwent freeze-drying, and the resulting dried sample was scrutinized for structure using a SEM (Thermo Fisher Scientific Phenom P-series) at magnifications ranging from 10,000 to 30,000x.

Cell proliferation analysis and half-maximal inhibitory concentration (IC)-50 determination

To determine the IC_{50} value, MCF-7 cells (5,000/well) were plated in a 96-well format. Following a 24 hr incubation, cell groups were subjected to treat with either DMSO (control) or AuNPs diluted in DMSO at the varying concentrations (25, 50, 100 µg/mL) for an additional 48 hr. Post-incubation, 10 µL of 12 mM MTT solution was introduced to each well, followed by a 3 hr incubation period, and the reaction was halted with the addition of 100 µL of STOP solution. Thorough mixing of the samples was ensured before measuring absorbance at 570 nm [29].

RNA isolation and gene expression analysis

MCF-7 cells were cultured in 6-well plates and subsequently categorized into four groups, each treated for 48 hr: the control group (DMSO-treated), positive control (treated with doxorubicin at 10 µg/mL), AuNP-I group (treated with AuNPs at 25 µg/mL), and AuNP-II group (treated with AuNPs at 50 µg/mL). Total RNA isolation was performed using the SV Total RNA Isolation System (Promega) following the manufacturer's protocol [30]. cDNA synthesis was conducted using ReverTra Ace qPCR RT Master Mix (Toyobo) according to the manufacturer's protocol, and q-PCR analysis was carried out using Thunderbird Next SYBR qPCR Mix (Toyobo). Forward and reverse primers for Cyclin D1 (*CCND1*), c-Myc (*MYC*), and β-actin (*ACTB*) were designed using Primer3Plus and obtained from Genebank (https://www.ncbi.nlm.nih.gov/) (Table 1). ACTB served as the internal control or reference gene. PCR reactions were conducted in a Rotor gene (MyGo Pro) thermocycler. The fold change in mRNA expression was calculated using the formula below:

Table 1. Forward and reverse primers sequences

Gene	Primer Forward (5'→3')	Primer Reverse (5'→3')
CCND1	AACTACCTGGACCGCTTCCT	CCACTTGAGCTTGTTCACCA
MYC	GGAGGAACAAGAAGATGAGG	GTAGTTGTGCTGATGTGTGG
ACTB	CCACACTGTGCCCATCTA CG	CAACTTCTGCCTTTGGCTTC

$$2^{-((Ctg-Cct)-average\ of\ Cct)}$$

Description:
Ct : Cycle threshold
Ctg : target gene
Cct : control gene

Statistical analysis

The data were acquired and presented as mean ± SD. Statistical analysis was conducted with GraphPad Prism 8, including a Shapiro-Wilk test (α>0.05) to assess data normality. Subsequent analyses were performed using either parametric or nonparametric methods based on the normality of the data.

RESULTS

Synthesis and characterization of AuNPs

The successful formation of AuNPs was visually confirmed by the emergence of a distinct purple color upon the mixing of the plant extract with $HAuCl_4$ solution (Fig. 1A). In the synthesis

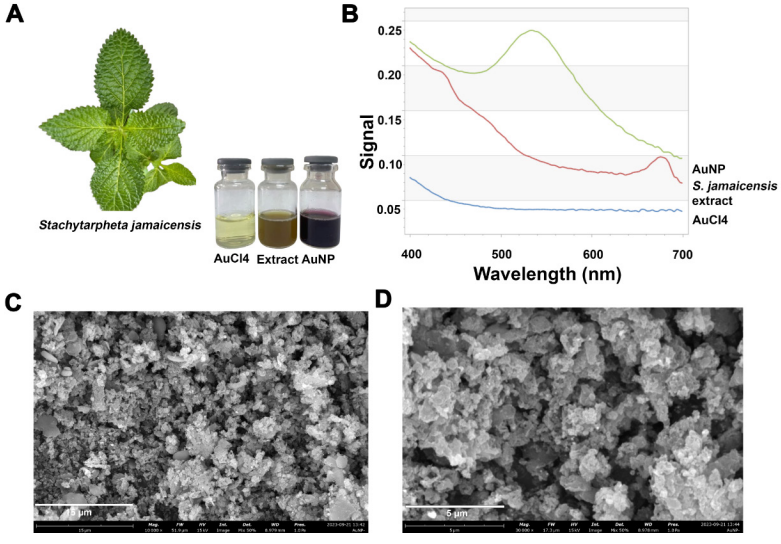

Fig. 1. Synthesis and characterization of AuNPs with *S. jamaicensis* extract. (A) *S. jamaicensis* leaves and color changes during synthesis AuNPs, and characterization of AuNPs using Uv-Vis spectrophotometry (B) and SEM with 10.000x (C) and 30.000x magnification (D)

process, the plant extract served as a potent reducing agent, effectively converting Au3+ to Au0. The resulting colloidal solutions underwent thorough examination using UV-vis spectroscopy, as illustrated in Fig. 1B. Notably, the absorption peaks of the AuNPs manifested within the wavelength range of 520-540 nm, consistent with the characteristic surface plasmon resonance (SPR) of AuNPs, typically observed around 520 nm and influenced by its size [31]. To further elucidate the morphology of AuNPs, SEM imaging was conducted, providing valuable insights into their structural features. As depicted in Fig. 1C, SEM images offer a clear visualization of AuNPs synthesized utilizing *S. jamaicensis* leaf extract. The observed accumulation of AuNPs reinforces the successful and controlled biosynthesis of AuNPs through this eco-friendly and efficient method.

FT-IR analysis was employed to discern potential bio-reducing biomolecules within the extract [26]. The identification of functional groups on the surface of synthesized AuNPs was conducted through FT-IR measurements, with the resulting spectra of both AuNPs and *S. jamaicensis* extract presented in Fig. 2A. The key peaks in the *S. jamaicensis* extract were observed at 3466, 1790, 1638, 1556, 964, and 571 cm^{-1}. Specifically, the peak at 3466 cm^{-1} signifies the presence of OH groups, encompassing both phenolic and aliphatic hydroxyl functionalities. The peak at 1790 cm^{-1} corresponds to the C=O stretching of acid halides, while the peak at 1638 cm^{-1} is indicative of C=C stretching in alkene groups. The presence of lignin, associated with the vibration of the aromatic skeleton C=C, is highlighted by the peak at 1556 cm^{-1} [32]. Additionally, peaks at 964 cm^{-1} correspond to the C=C bending of alkene, while those at 571 cm^{-1} represent the C-I stretching of halo compounds. These distinctive peaks collectively contribute to the comprehensive characterization of the identified biomolecules involved in the reduction process.

The FT-IR spectrum of AuNPs revealed distinct peaks at 3466, 2114, 1793, 1634, 1466, 1127, 1100, and 629 cm^{-1}. A minor wavelength shift was observed in the peaks corresponding to the functional groups present in the extract before and after the formation of AuNPs, suggesting an interaction between these functional groups and the NPs. The broad peak at 3466 cm^{-1} signifies the characteristic presence of phenolic compounds, while the peak at 2114 cm^{-1} indicates the representation of a simple gold monocarbonyl species. Additionally, bands at 1634 cm^{-1}, 1127 cm^{-1}, and 1100 cm^{-1} correspond to the alkene group, tertiary alcohol, and aliphatic ether of the plant extract, respectively. These findings suggest that the *S. jamaicensis* extract not only facilitates the reduction of gold ions but also plays a crucial role in stabilizing the resulting AuNPs.

The particle size distributions obtained from PSA results for *S. jamaicensis* extract, HAuCl4 and colloidal AuNPs are presented in Fig. 2B-D, respectively. The average particle sizes measured for *S. jamaicensis* extract, HAuCl4, and AuNPs colloids are 34.1, 224.3, and 60.3 nm, respectively. This outcome serves as compelling evidence of the *S. jamaicensis* extract's capability to effectively reduce HAuCl4 to AuNPs, as demonstrated by the considerable reduction in particle size.

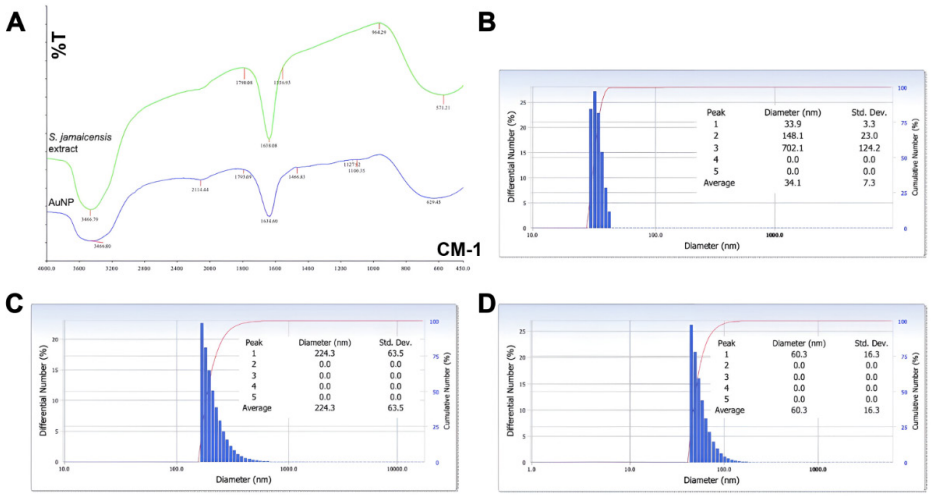

Fig. 2. Characterization of AuNPs using FT-IR (A) and PSA (B-D).

Half-maximal inhibitory concentration (IC_{50}) of AuNPs

The IC_{50} of AuNPs was determined through a comprehensive assessment involving three dose variations (25, 50, and 100 µg/mL) and a single incubation time (48 hr). The MTT assay was employed as the measurement method, and the obtained optical density (OD) results enabled the calculation of cell viability percentages. Utilizing the data on percent cell viability, the IC_{50} value was determined, representing the dose required for AuNPs to induce a 50% reduction in cell population from the initial number. The IC_{50} results for AuNPs are depicted in Fig. 3. In the MCF7 cell culture, following a 48-hr incubation period, AuNPs demonstrated a notable inhibition of cell viability ranging from 37.42% to 55.66%, ultimately yielding an IC_{50} value of 19.53 µg/mL. These findings underscore the significant anti-proliferative effects of AuNPs and provide valuable insights into their potential therapeutic application in cancer treatment.

Effect of AuNPs on *CCND1* and *MYC* expression

A predominant cause of cancer malignancies stems from the heightened expression of oncogenes within cells. The proteins encoded by the *MYC* gene play a pivotal role in governing the cell cycle and cell proliferation by regulating key genes associated with the cell cycle, including cyclin, CDKs, and transcription factor E2F [33]. Expression values, representing mRNA levels normalized to the control group expression, were determined through triplicate experiments with comparisons made using the housekeeping gene *ACTB*. The error bars in the figures illustrate the mean ± SD.

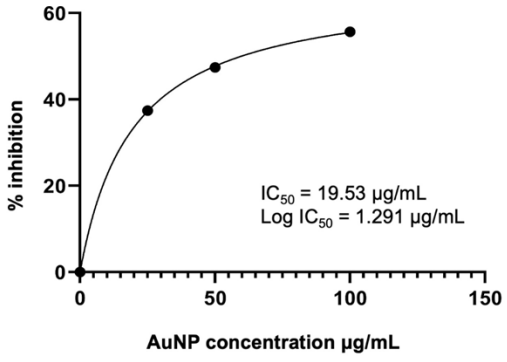

Fig. 3. IC_{50} of AuNPs from *S. jamaicensis* extract against MCF7 cell line after 48 hr of treatment

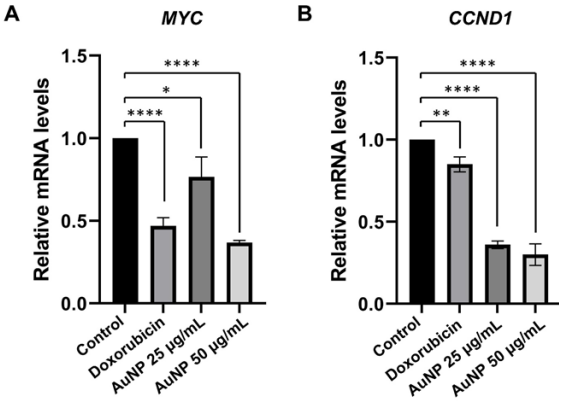

Fig. 4. mRNA expression of MYC (A) and CCND1 (B) in MCF7 cell line following treatment with AuNPs for 48 hours. Doses of AuNP: 25 µg/mL and 50 µg/mL

In Fig. 4A, it is evident that treatment with AuNPs led to a significant reduction in the mRNA levels of the *MYC* oncogene. Specifically, at a dose of 25 µg/mL, there was a 24% decrease in *MYC* expression (0.76 ± 0.12-fold), while the 50 µg/mL dose resulted in a substantial 63% reduction in *MYC* expression (0.37 ± 0.01-fold). Fig. 4B further highlights the efficacy of AuNPs in diminishing the expression of Cyclin D1 (*CCND1*). The 25 µg/mL dose of AuNPs demonstrated a noteworthy 64% reduction in the *CCND1* expression (0.36 ± 0.02-fold), while the 50 µg/mL dose achieved a 70% decrease in *CCND1* expression (0.3 ± 0.19-fold). These findings underscore the potential of AuNPs to modulate the expression of critical oncogenes, providing valuable insights into their anti-proliferative mechanisms in cancer cells.

DISCUSSION

In recent decades, advancements in nanotechnology, particularly with AuNPs, have paved the way for numerous bioscience applications, especially in the detection of biomarkers, leveraging the distinctive optical properties of colloidal AuNPs. This study explores the potential of the *S. jamaicensis* plant extract as a reducing agent to facilitate the reduction of gold ions, leading to the aggregation and growth of AuNPs. As noted by Wuithschick et al., the emergence of a blue/purple color during synthesis is attributed to the adsorption of NaAuCl4 on the nanoparticle surface, influencing the surface chemistry and dielectric constant of the surrounding medium. The reduction of NaAuCl4 occurs rapidly, resulting in light extinction by AuNPs and generating colors spanning from

red and purple to blue and ultimately, brown [34]. These color variations are contingent upon factors such as particle size, shape, structure, and aggregation state, constituting a phenomenon known as localized surface plasmon resonance, wherein the surface electrons of AuNPs oscillate in resonance with incident light [35-37].

Our results align with Zuber et al.'s findings, which observed a change in the solution color and the appearance of a plasmon peak between 520–540 nm, as a sign of AuNP formation [38]. Validated by UV-vis spectroscopy, our study confirms the reaction completion after 24 hr, revealing a plasmonic peak at 520-540 nm. This substantiates the successful synthesis of AuNPs and highlights their potential applications in biomedical and bioscience applications.

In our current study, we explored the potential of *S. jamaicensis* extract in synthesizing AuNPs. SEM studies unveiled the morphology of AuNPs with a measured average particle size of 60.3 nm as determined by PSA. AuNPs with varying sizes exhibit distinct absorption spectra, with maximum absorption peaks typically falling within the range of 520–530 nm when the diameters range from 12 to 41 nm. The observed purple color of the green0synthesized AuNPs and the larger average nanoparticle diameter aligns with the previous findings, where colors transition from orange to red, and then, to purple with increasing nanoparticle sizes [39]. These results support the findings of our study, where the color of the AuNPs solution is deep purple, and the average diameter is bigger than 41 nm.

The synthesis process involved mixing Au metal precursor solution with *S. jamaicensis* extract, which acted as both a reducing and stabilizing agent. FT-IR analysis revealed the components of the plant extract responsible for the reduction and stabilization processes. Consistent with a previous study on AuNPs synthesized from Abies spectabilis extract, our FT-IR data (Fig. 2A) indicated the involvement of multiple compounds from *S. jamaicensis* extract in the synthesized AuNPs, suggesting their potential role as capping agents [28, 40].

The cytotoxic effects of AuNPs have been documented in the various cancer cell lines, including Hep2, MDA-MB-231, Caco-2, and T24 cancer cells [28, 41-43]. The observed cytotoxicity of AuNPs is intricately linked to factors such as NP size, surface charge, and functional groups [44]. Smaller AuNPs, characterized by increased tissue distribution, deeper penetration into specific tissues, enhanced cellular uptake, and heightened toxic effects, have been associated with these cytotoxic outcomes [17]. Taking these factors into consideration, our investigation revealed a notable decrease in cell viability following treatment with synthesized AuNPs at relatively low concentrations, resulting in an IC_{50} value of 19.53 µg/mL in the MCF7 cell line. In contrast, spherical AuNPs (21 nm) stabilized by citrate showed no toxic effects on human breast cancer cell lines (MCF-7) or human prostate cancer cell lines (PC-3), as reported by the previous studies. Additionally, it has been documented that spherical AuNPs (10–50 nm) stabilized by citrate exhibited non-toxicity towards human leukemic cells (K562) [45]. This study clearly illustrates that the photochemicals found in *S. jamaicensis* serve as an effective anticancer coating on AuNPs.

To gain insights into the mechanism behind the observed reduction in the cell viability, we examined the mRNA expression of c-Myc and Cyclin D1. The c-Myc oncogene, frequently deregulated in human cancers, plays a pivotal role in cell cycle progression, proliferation, apoptosis, and cellular transformation [46, 47]. Protein c-Myc acts as a transcription factor, and when it binds to the CACGTG (E-box), the resulting Myc–Max dimeric complex brings in chromatin-modifying complexes such as GCN5, TIP60, TIP48, and TRRAP. This recruitment leads to the activation of transcription, with GCN5 and TIP60 functioning as histone acetyltransferases, TIP48 as an ATP-binding protein, and TRRAP as a transactivation-associated protein [48]. One of many c-Myc target gene is Cyclin D1, an important regulator of cell cycle progression.

Cyclin D1 is encoded by the CCND1 gene, which forms complexes with either CDK4 or CDK6. These complexes phosphorylate and deactivate retinoblastoma (Rb), promoting the progression of the cell cycle from G1 to S phase. Changes such as mutations, amplification, or overexpression of cyclin D1 can disrupt normal cell cycle progression, potentially playing a role in the development of tumors [49]. The coordination of c-Myc with Cyclin D1 not only expedites tumor formation but may also drive tumor progression towards a more aggressive phenotype. Consequently, targeting c-Myc and Cyclin D1 represents a promising strategy for cancer therapy [50]. Our results

demonstrated that AuNPs synthesized using *S. jamaicensis* extract significantly reduced c-Myc and Cyclin D1 mRNA levels in MCF7 cells. This reduction in the c-Myc expression is particularly noteworthy, as it is associated with inhibited cell proliferation, induction of apoptosis, decreased tumor angiogenesis, and impaired invasion and metastasis, a promising outcome with implications for potential cancer therapy strategies [48, 50-52]. These findings collectively underscore the multifaceted potential of AuNPs synthesized with *S. jamaicensis* extract in cancer therapeutics.

CONCLUSION

In conclusion, the biosynthesis of AuNPs using *S. jamaicensis* leaves aqueous extract presents a breakthrough in terms of affordability, speed, and safety, eliminating the need for toxic chemicals. The SEM imaging showcased the formation of AuNPs, while FT-IR analysis indicated a surface coverage of biomolecules, particularly phenolics compounds from the plant extract. Significantly, these AuNPs exhibited remarkable anticancer properties, evidenced by an impressive IC_{50} value of 19.53 µg/mL against the MCF7 cell line. Furthermore, the mechanistic insights revealed a reduction in cell viability associated with the downregulation of key oncogenes, *MYC* and *CCND1*, in breast cancer. This promising anticancer potential paves the way for future investigations, particularly through in-vivo studies, to comprehensively assess the therapeutic efficacy and safety of AuNPs. The findings not only underscore the potential of AuNPs as a valuable tool in cancer treatment but also emphasize the importance of eco-friendly and cost-effective synthesis methods for nanomaterials with biomedical applications.

ACKNOWLEDGMENTS

This study was financially supported by SATU-JRS research funding 2023 (grant number: 1602/UN3.LPPM/PT.01.03/2023).

ETHICS APPROVAL

This article does not contain any studies on human or animals.

CONFLICT OF INTEREST

There are no potential conflicts of interest.

REFERENCES

1. Liu L, Corma A. Metal catalysts for heterogeneous catalysis: from single atoms to nanoclusters and nanoparticles. Chem Rev. 2018; 118(10): 4981-5079.
2. Gao P, Pan W, Li N, Tang B. Boosting cancer therapy with organelle-targeted nanomaterials. ACS Appl Mater Interfaces. 2019;11(30): 26529-2658.
3. Wang M, Mohanty SK, Mahendra S. Nanomaterial-supported enzymes for water purification and monitoring in point-of-use water supply systems. Acc Chem Res. 2019; 52(4): 876-885.
4. Liu XY, Wang JQ, Ashby CR Jr, Zeng L, Fan YF, Chen ZS. Gold nanoparticles: synthesis, physiochemical properties and therapeutic applications in cancer. Drug Discov Today. 2021; 26(5): 1284-1292.
5. Alex S, Tiwari A. Functionalized gold nanoparticles: synthesis, properties and applications: a review. J Nanosci Nanotechnol. 2015; 15(3): 1869-94.
6. Sarfraz N, Khan I. Plasmonic gold nanoparticles (AuNPs): properties, synthesis and their advanced energy, environmental and biomedical applications. Chem Asian J. 2021; 16(7): 720-42.
7. Son D, Bao Z. Correction to nanomaterials in skin-inspired electronics: toward soft and robust skin-like electronic nanosystems. ACS Nano. 2018; 12(12): 12943.
8. Boruah JS, Devi C, Hazarika U, Reddy PVB, Chowdhury D, Barthakur M, et al. Green synthesis of gold nanoparticles using an antiepileptic plant extract: in vitro biological and photo-catalytic activities. RSC Adv. 2021; 11(45): 28029-41.
9. Mostafa EM, Abdelgawad MA, Musa A, Alotaibi NH, Elkomy MH, Ghoneim MM, et al. Chitosan silver and gold nanoparticle formation using endophytic fungi as powerful antimicrobial and anti-biofilm potentialities. Antibiotics (Basel). 2022; 11(5).
10. Bharadwaj KK, Rabha B, Pati S, Sarkar T, Choudhury BK, Barman A, et al. Green synthesis of gold nanoparticles using plant extracts as beneficial prospect for cancer theranostics. Molecules. 2021; 26(21).
11. Rajasekar T, Karthika K, Muralitharan G, Maryshamya A, Sabarika S, Anbarasu S, et al. Green synthesis of gold nanoparticles using extracellular metabolites of fish gut microbes and their antimicrobial properties. Braz J Microbiol. 2020; 51(3): 957-67.
12. Timoszyk A, Grochowalska R. Mechanism and antibacterial activity of gold nanoparticles (aunps) functionalized with natural compounds from plants. Pharmaceutics. 2022; 14(12).
13. Muddapur UM, Alshehri S, Ghoneim MM, Mahnashi MH, Alshahrani MA, Khan AA, et al. Plant-based synthesis of gold nanoparticles and theranostic applications: a review. Molecules. 2022; 27(4).
14. Akrami M, Samimi S, Alipour M, Bardania H, Ramezanpour S, Najafi N, et al. Potential anticancer activity of a new pro-apoptotic peptide-thioctic acid gold nanoparticle platform. Nanotechnology. 2021; 32(14): 145101.
15. Maity R, Chatterjee M, Banerjee A, Das A, Mishra R, Mazumder S, et al. Gold nanoparticle-assisted enhancement in the anti-cancer properties of theaflavin against human ovarian cancer cells. Mater Sci Eng C Mater Biol Appl. 2019; 104:109909.
16. Adhikari C, Das A, Chakraborty A. Controlled release of a sparingly water-soluble anticancer drug through pH-responsive functionalized gold-nanoparticle-decorated liposomes. Chemphyschem. 2015; 16(4): 866-71.
17. Peng J, Liang X. Progress in research on gold nanoparticles in cancer management. Medicine (Baltimore). 2019; 98(18): e15311.
18. Lim ZZ, Li JE, Ng CT, Yung LY, Bay BH. Gold nanoparticles in

cancer therapy. Acta Pharmacol Sin. 2011; 32(8): 983-90.
19. Singh M, Harris-Birtill DC, Markar SR, Hanna GB, Elson DS. Application of gold nanoparticles for gastrointestinal cancer theranostics: A systematic review. Nanomedicine. 2015; 11(8): 2083-98.
20. Liew PM, Yong YK. *Stachytarpheta jamaicensis* (L.) Vahl: from traditional usage to pharmacological evidence. Evid Based Complement Alternat Med. 2016; 2016:7842340.
21. Jagadish NG. Evaluation of analgesic activity of different extracts of *Stachytarpheta indica* L. (Vahl). IEEE Trans Biomed Eng. 2008; 3: 229-33.
22. Sulaiman MR, Zakaria ZA, Chiong HS, Lai SK, Israf DA, Azam Shah TM. Antinociceptive and anti-inflammatory effects of *Stachytarpheta jamaicensis* (L.) Vahl (Verbenaceae) in experimental animal models. Med Princ Pract. 2009; 18(4): 272-9.
23. Ruma OC, Zipagang TB. Determination of secondary metabolites and antibacterial property of extract from the leaves of *Stachytarpheta jamaicensis* (L.) Vahl. J Med Plants Stud. 2015; 3(4): 79-81.
24. Jalalvand AR, Zhaleh M, Goorani S, Zangeneh MM, Seydi N, Zangeneh A, et al. Chemical characterization and antioxidant, cytotoxic, antibacterial, and antifungal properties of ethanolic extract of *Allium Saralicum* R.M. Fritsch leaves rich in linolenic acid, methyl ester. J Photochem Photobiol B. 2019; 192: 103-12.
25. Wu G, Liu X, Zhou P, Wang L, Hegazy M, Huang X, et al. A facile approach for the reduction of 4-nitrophenol and degradation of congo red using gold nanoparticles or laccase decorated hybrid inorganic nanoparticles/polymer-biomacromolecules vesicles. Mater Sci Eng C Mater Biol Appl. 2019; 94: 524-33.
26. Elia P, Zach R, Hazan S, Kolusheva S, Porat Z, Zeiri Y. Green synthesis of gold nanoparticles using plant extracts as reducing agents. Int J Nanomedicine. 2014; 9: 4007-21.
27. Aljabali AAA, Akkam Y, Al Zoubi MS, Al-Batayneh KM, Al-Trad B, Abo Alrob O, et al. Synthesis of gold nanoparticles using leaf extract of *ziziphus zizyphus* and their antimicrobial activity. Nanomaterials (Basel). 2018; 8(3).
28. Wu T, Duan X, Hu C, Wu C, Chen X, Huang J, et al. Synthesis and characterization of gold nanoparticles from *Abies spectabilis* extract and its anticancer activity on bladder cancer T24 cells. Artif Cells Nanomed Biotechnol. 2019; 47(1): 512-23.
29. Dewi FRP, Shoukat N, Alifiyah NI, Wahyuningsih SPA, Rosyidah A, Prenggono MD, et al. Increasing the effect of annonacin using nanodiamonds to inhibit breast cancer cells growth in rats (*Rattus norvegicus*)-Induced breast cancer. Heliyon. 2022; 8(11): e11418.
30. Nisa N, Wahyuningsih SPA, Darmanto W, Purnama PR, Dewi FRP, Soegiarti T, et al. Effect of the ethanol extract of red okra pods (*Abelmoschus esculentus* (L.) Moench) to inhibit cervical cancer cells growth through cell cycle-associated oncogenes. Scientifica (Cairo). 2022; 2022: 1094771.
31. Huang W, Wang L, Long D, Liu X. Colorimetric determination and recycling of gold(III) ions using label-free plasmonic H(0.3)MoO(3) nanoparticles. Mikrochim Acta. 2023; 190(6): 245.
32. Costa LASA DJ, Gomes GVP, da Silva JBA, Fonseca AF, Druzian JI. Extraction and characterization of nanocellulose from corn stover. Materials Today: Proceedings 2015; 2: 287-94.
33. Garcia-Gutierrez L, Delgado MD, Leon J. MYC oncogene contributions to release of cell cycle brakes. Genes (Basel). 2019; 10(3).
34. Wuithschick M, Birnbaum A, Witte S, Sztucki M, Vainio U, Pinna N, et al. Turkevich in new robes: key questions answered for the most common gold nanoparticle synthesis. ACS Nano. 2015; 9: 7052-71.
35. Slepicka P, Slepickova Kasalkova N, Siegel J, Kolska Z, Svorcik V. Methods of gold and silver nanoparticles preparation. Materials (Basel). 2019; 13(1).
36. Wagner FE, Haslbeck S, Stievano L, Calogero S, Pankhurst QA, Martinek KP. Before striking gold in gold-ruby glass. Nature. 2000; 407(6805): 691-2.
37. Cardell C, Guerra I. Natural corrosion-induced gold nanoparticles yield purple color of Alhambra palaces decoration. Sci Adv. 2022; 8(36): eabn2541.
38. Zuber A, Purdey M, Schartner E, Forbes C, van der Hoek B, Giles D, et al. Detection of gold nanoparticles with different sizes using absorption and fluorescence based method. Sens Actuators Rep. 2016; 227: 117-27.
39. He YQ, Liu SP, Kong L, Liu ZF. A study on the sizes and concentrations of gold nanoparticles by spectra of absorption, resonance Rayleigh scattering and resonance non-linear scattering. Spectrochim Acta A Mol Biomol Spectrosc. 2005; 61(13-14): 2861-6.
40. Varshney R, Bhadauria S, Gaur MS. Biogenic synthesis of silver nanocubes and nanorods using sundried Stevia rebaudiana leaves. Adv Mater Lett. 2010; 1: 232-7.
41. Priya MRK, Iyer PR. Antiproliferative effects on tumor cells of the synthesized gold nanoparticles against Hep2 liver cancer cell line. Egypt Liver J. 2020; 10(1): 15.
42. Majoumouo MS, Sharma JR, Sibuyi NRS, Tincho MB, Boyom FF, Meyer M. Synthesis of biogenic gold nanoparticles from *terminalia mantaly* extracts and the evaluation of their *in vitro* cytotoxic effects in cancer cells. Molecules. 2020; 25(19).
43. Jeyarani S, Vinita NM, Puja P, Senthamilselvi S, Devan U, Velangani AJ, et al. Biomimetic gold nanoparticles for its cytotoxicity and biocompatibility evidenced by fluorescence-based assays in cancer (MDA-MB-231) and non-cancerous (HEK-293) cells. J Photochem Photobiol B. 2020; 202: 111715.
44. Kus-Liskiewicz M, Fickers P, Ben Tahar I. Biocompatibility and cytotoxicity of gold nanoparticles: recent advances in methodologies and regulations. Int J Mol Sci. 2021; 22(20).
45. Vijayakumar S, Ganesan S. In vitro cytotoxicity assay on gold nanoparticles with different stabilizing agents. J Nanomater. 2012; 2012(734398).
46. Meyer N, Penn LZ. Reflecting on 25 years with MYC. Nat Rev Cancer. 2008; 8(12):976-90.
47. Dang CV, O'Donnell KA, Zeller KI, Nguyen T, Osthus RC, Li F. The c-Myc target gene network. Semin Cancer Biol. 2006;16(4): 253-64.
48. Chen H, Liu H, Qing G. Targeting oncogenic Myc as a strategy for cancer treatment. Signal Transduct Target Ther. 2018; 3:5.
49. Montalto FI, De Amicis F. Cyclin D1 in cancer: a molecular connection for cell cycle control, adhesion and invasion in tumor and stroma. Cells. 2020; 9(12).
50. Liao DJ, Thakur A, Wu J, Biliran H, Sarkar FH. Perspectives on c-Myc, Cyclin D1, and their interaction in cancer formation, progression, and response to chemotherapy. Crit Rev Oncog. 2007; 13(2): 93-158.
51. Gao FY, Li XT, Xu K, Wang RT, Guan XX. c-MYC mediates the crosstalk between breast cancer cells and tumor microenvironment. Cell Commun Signal. 2023; 21(1): 28.
52. Jeffreys SA, Becker TM, Khan S, Soon P, Neubauer H, de Souza P, et al. Prognostic and predictive value of ccnd1/cyclin d1 amplification in breast cancer with a focus on postmenopausal patients: a systematic review and meta-analysis. Front Endocrinol (Lausanne). 2022; 13: 895729.